NUMERICAL SIMULATION OF THE CO_2-DIFFUSION EFFECT ON LOW TURBULENT MIXED CONVECTION IN A VENTILATED ROOM HEATED BY THE BOTTOM

Lounes KOUFI [1]***, Zohir YOUNSI*** [2]***, Hassane NAJI*** [2,*]

[1] LMDC, INSA/UPS Génie Civil, 135 Avenue de Rangueil, F-31077 Toulouse, France

[2] Univ. Artois, Univ. Lille, Yncréa-HEI, IMT-Douai, ULR 4515-LGCgE, F-62400 Béthune, France

[*] Corresponding author; E-mail: *hassane.naji@univ-artois.fr*

A double-diffusive mixed convection within low-turbulent regime in a ventilated cavities filled with an air-CO_2 mixture and heated from below has been numerically investigated. The lower wall was sustained at a uniform temperature and CO_2-concentration. The vertical and upper walls were kept at external temperature and CO_2-concentration. To analyze the behavior of flow, the ventilation effectiveness for temperature distribution and removal of CO_2-contaminant, four configurations were dealt. These differ from each other by the location of the mixture inlet and outlet gaps. Likewise, three CO_2-concentrations were considered (10^3, $2x10^3$ and $3x10^3$ ppm) to investigate the influence of the CO_2-diffusion on the ventilation effectiveness. The numerical simulations were performed by considering closed Reynolds averaged-Navier-Stokes (RANS) equations using the Re-Normalization Group k-ε model. The governing equations' set was then solved using the finite volume method, in which the pressure-velocity coupling was handled using the SIMPLEC algorithm. Validation of the numerical model was achieved by comparing our results with available experimental data. The obtained results indicate that the CO_2-diffusion effect on the air movement and the ventilation effectiveness for temperature distribution can be neglected in the present study. However, the CO_2-diffusion remains a key parameter in terms of indoor air quality index. Also, it was found that one of the studied configurations provides a better ventilation effectiveness to remove heat and CO_2-contaminant, and insures a homogeneous temperature and CO_2-concentration in the occupied zone. The three other configurations maintain an acceptable level of heat and can be used in temperate climate to ensure good indoor air quality.

Key words*: heat transfer, turbulent mixed convection, contaminant diffusion, ventilated room, numerical simulation.*

1. Introduction

Over the last few decades, indoor air pollution has become a major concern and presents potential risks to public health. To deal with this situation, air renewal is one of the promising solutions. To achieve an efficient air renewal, it is essential to improve our knowledge of how ventilation distributes fresh air and how pollutants are transported within indoor spaces. Nowadays, indoor air quality (IAQ) has become of greater concern due to the long time periods people stay inside

confined spaces. It has been mentioned that we spend more than 90% of our time in closed spaces such as homes, schools, offices, transports or shopping centers [1]. Furthermore, contaminant levels within indoor environment are typically much higher than those of outdoor environment [2]. More and more polluted products are being emitted by used building materials and furnishings, consumer and decoration products. Further, since the 1973 oil crisis, indoor spaces have been sealed and narrowed to reduce the energy consumption involved with heat losses through the envelopes [3]. Though such a development has reduced costs associated with energy consumption, it has also generated other issues such as confinement and poor air quality [3].

To avoid these constraints related to the air tightness, the ventilation is among the promising solutions. Its main objective is to provide a healthy environment by supplying unpolluted fresh air and clearing out contaminants. Moreover, the indoor airflow is an important element for thermal comfort, which depends on several parameters such as air temperature, radiant temperature, humidity, air velocity etc. Therefore, it is required to have an idea of how the fresh air is distributed indoors. Many investigations according to the characteristics of indoor airflows so as to control temperature distribution and pollutant removal have been documented [4-9], to name a few.

In indoor environments, it is well known that two physical phenomena occur, namely the natural convection generated by the buoyancy forces induced by temperature and pressure gradients, and the forced convection associated to the mechanical ventilation. The competition between buoyancy forces and external forces can generate mixed convection. Moreover, in the presence of concentration gradients, indoor airflow becomes complex and is governed by double-diffusive mixed convection effects.

As is well known, double-diffusive mixed convection airflows are encountered in many applications (i.e. engineering and geophysical). This includes room ventilation, nuclear reactors cooling, solar ponds, lakes and reservoirs, solar collectors, cooling of electronic devices, crystal growth [10-13]. Literature review highlights that various researchers have investigated the mixed convective flows in ventilated cavities, using analytical, experimental, and numerical approaches.

In what follows, we briefly describe some work related to the turbulent regime in ventilated cavities with contaminant gradients. Serrano-Arellano et al. [5] numerically conducted a study of heat and mass transfers induced by conduction, convection and radiation inside different ventilated cavities filled with an air-CO_2 mixture, which differ by the location of the mixture outlet opening. They reported that, in general, to obtain the advised values of temperature and CO_2-concentrations, it was sound to consider mixed convection at Reynolds number from 10^4. Di Liu et al. [6] numerically performed a study of heat and mass transfer by turbulent mixed convection in a 3D-ventilated cavity having an air conditioner window equipped with three slots for blowing, extracting and recirculation. They stated that contaminant reduction rates can be achieved either by increasing fresh air ratio or Re number, increasing the supply air flow, or reducing the heating source. Cao and Meyers [7] have developed a fast approach based on low-dimensional models for ventilation monitoring and control. They have shown that the flow equations decouple from the concentration equation when the mass air flow/pollutant mass flow ratio is sufficiently large. In another study [8], they investigated the turbulent inlet quantities effect on indoor airflow parameters and pollutant dispersion using two turbulence models (low-Reynolds number k-ε and SST k-ω models). They found that the turbulent length scales variation at the inlet induce small changes in the indoor flow field. In addition, regarding the pollutants dispersion, they indicated that the inlet turbulent quantities fluctuation leads to differences in pollutant

concentration up to 20%. Deng et al. [9] numerically analyzed the air change rates effect on indoor CO_2 diffusion and removal inside a 3D-ventilated room. The authors stressed that the results obtained would be of great interest for practical applications to design and control ventilation systems from a health and energy efficiency perspective. Krajčík et al. [14] experimentally conducted a study on air distribution, ventilation effectiveness and thermal environment inside a room heated and ventilated by hot air supplied by a mixing ventilation system. Comparing with the case of underfloor heating, these authors found that the cooling supply air mixed well and created very uniform conditions with proper ventilation efficiency when the underfloor heating system was used. Rodríguez-Muñoz et al. [15] analyzed the effect of heat and CO_2 emitted by a human being exhibited to mixed turbulent convection with radiation in a naturally ventilated room. They found that the natural ventilation reduces the average room temperature by about 4°C to 5.5°C, while radiation rises it between 0.2 °C and 0.4 °C. Serrano-Arellano et al. [16] performed a study to define an optimal configuration based on the location of air outlet port allowing better CO_2-contaminant removal from 2D-ventilated cavities with the air inlet port located on the lower right vertical wall. The found that the case where the air outlet port is at the top side removes a greater amount of contaminant for a $Re = 5x10^3$, which had an effect on energy savings. In transient regime, Serrano-Arellano et al. [17] numerically studied double-diffusive convection with conduction and radiation conditions inside a ventilated cavity filled with an air-CO_2 mixture where an air outlet gap was set close to the heat and contaminant sources. They reported that the advised thermal and air quality parameters were met within 15s for $Re = 1x10^4$.

Based on the literature review up-reported, it appeared that research on the ventilation systems' ability to ensure better temperature distribution and better CO_2-diffusion in environments ventilated interiors operating with low Reynolds numbers remain scarce. Thereby, it seems useful to conduct a numerical study to predict the airflow behavior inside ventilated rooms subjected to temperature and concentration gradients as a first approximation. The objectives here are twofold: ***a***) to numerically perform a study of the low-turbulent double-diffusive mixed convection from a ventilated cavity heated from below, and ***b***) to assess the CO_2-diffusion effect on the airflow behaviour, the temperature and concentration distributions, and the IAQ.

2. Computational analysis

2.1. Physical domain

Fig. 1 shows the investigated configuration (1.04x1.04 m^2, i.e. length and height) with the Cartesian coordinate system. We consider this cavity because of the interesting experimental data availability [18]. Here, the working fluid is an air-CO_2 mixture. The bottom wall is subjected to uniform temperature (T_H) and CO_2-concentration (C_H). External conditions (i.e. temperature (T_C) and CO_2-concentration (C_L)) are applied to the other walls, with $T_H > T_C$ and $C_H > C_L$. The air-CO_2 mixture is

renewed by providing fresh air from outside (T_C and C_L) through an opening mounted at the top of the left wall. The polluted air leaves the cavity through an opening at the bottom of the right side. The air inlet velocity is fixed at 0.57 ms^{-1}, which leads to Re = 706. The considered thermal Rayleigh number is $2.62x10^9$ (with T_H = 308.5 K). The Lewis number corresponding to considered thermal and mass diffusivities (α and D) is equal to 1.47. The thermo-physical properties of air-CO_2 mixture were achieved by using recommended relationships by Poling et al. [19].

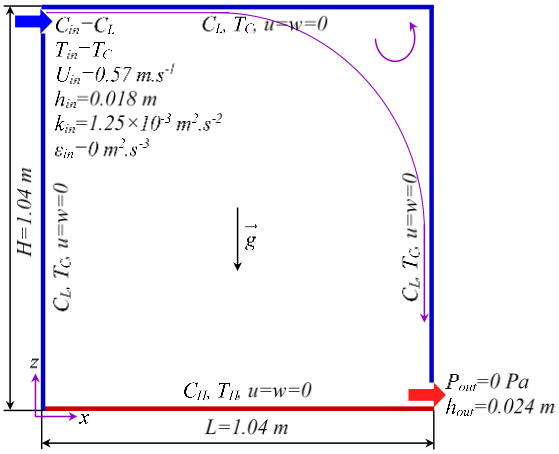

Figure 1. Ventilated cavity configuration with associated boundary conditions.

2.2. Governing equations

To analyze the steady state low-turbulent double-diffusive flow in the whole cavity, the commercially available CFD software scStream was used. The following assumptions were made-up: a) the flow is turbulent, fully developed and viscous; b) the air-CO_2 mixture is Newtonian and incompressible under the Boussinesq approximation; and c) the dissipation, pressure forces' work, and radiation are assumed to be negligible. In addition, the CO_2 concentration level is low (it is 0.04% lower compared to air). The RANS equations coupled to the RNG k-ε turbulence model having been deemed herein are those described in Ref. [20].

2.3. Boundary conditions

The appropriate boundary conditions (BCs) for the present problem are: u = w = 0 on the all solid surfaces, u = u_{in} and w = 0 ms^{-1} at the air inlet, $\partial(u,w)/\partial n = 0$ at the air outlet, n being the unit normal. As for thermal BCs, the temperature of the: air inlet is T_{in} = 288 K, floor is T_H = 308.5 K, other walls is T_C = 288 K. For the CO_2-contaminant, at inlet port is C_{in} = 350 ppm, at the floor is C_H (varied between 10^3 and $3x10^3$ ppm), at the other walls is C_L = 350 ppm. The boundary conditions for T and C at the outlet are Neumann conditions, i.e., $\partial T/\partial n = \partial C/\partial n = 0$. Regarding the turbulent quantities, their values are k_{in} = $1.25x10^{-3}$ m^2s^{-2} and ε_{in} = 0 m^2s^{-3} at the inlet port [18], while at the air outlet, $\partial k/\partial n = \partial \varepsilon/\partial n = 0$. At this port (outlet), an atmospheric pressure value has been set.

3. Numerical Procedure

3.1. Discretization

The above governing equations were solved numerically employing a finite-volume method. To avoid possible artificial diffusion, which is caused by truncation errors due to the discretization, a QUICK scheme and a second-order central differencing scheme were involved in approximating the advection and diffusion terms, respectively. Note that the pressure-velocity coupling was performed using the SIMPLEC algorithm, and that the numerical resolution was achieved using multiple-iteration constrained conjugate gradient. When the residual values of the different equations are sufficiently low for every control volume, overall convergence is achieved (10^{-8} for each variable). Table 1 shows the

results' convergence of heat balance at the last iteration of the computation. We find that the receiving and release heat are equivalent meaning, thereby, that convergence is reached.

Table 1. Heat receiving and release balances for the computation's last iteration with $C_H = 3x10^3$ *ppm*.

Heat receiving balance (*W*)	Heat release balance (*W*)	Total (*W*)
$2.48x10^{-2}$	$2.48x10^{-2}$	0.00

To ensure that the results are grid-independent and well-resolved, the simulations were repeated with different fine levels of meshing. It was determined that there were no noticeable differences in the solutions when the number of cells is around 196x196 cells or greater. Table 2 illustrates the relative error of mean temperature and concentration (T_m and C_m), maximum and minimum velocity components (at $X = 0.5$ or $Z = 0.5$), and their locations (X or Z) of the 196x196-grid. A maximum deviation of 1.0% for all variables between meshes 196x196 and 216x216-grid was spotted.

Table 2. Relative errors between grids and 196*x*196-grid with $C_H = 3000$ *ppm*.

Grid	176*x*176	196*x*196	216*x*216
C_m (*ppm*)	836.06 (0.66%)	830.59	826.76 (0.46%)
T_m (*K*)	292.47 (0.00%)	292.47	292.47 (0.00%)
$u_{max}x10^{-1}$ at X = 0.5 (ms^{-1})	3.42 (1.72%)	3.48	3.51 (0.86%)
Z	0.99 (0.70%)	0.99	0.99 (0.00%)
$u_{min}x10^{-1}$ at X = 0.5 (ms^{-1})	-3.57 (0.56%)	-3.59	-3.59 (0.00%)
$Zx10^{-2}$	1.83 (0.00%)	1.83	1.84 (0.55%)
$w_{max}x10^{-1}$ at Z = 0.5 (ms^{-1})	3.09 (1.59%)	3.14	3.16 (0.64%)
$Xx10^{-2}$	3.22 (6.27%)	3.03	3.00 (0.99%)
$w_{min}x10^{-1}$ at Z = 0.5 (ms^{-1})	-3.88 (0.51%)	-3.90	-3.91 (0.26%)
X	0.99 (0.00%)	0.99	0.99 (0.00%)

3.2. Numerical validation

To check and validate our approach, the ventilated cavity under thermal buoyancy force and low-turbulent regime reported by [18] was solved. To avoid overloading the text, note that the verification and validation processes have already been presented in previous work [21-24], with satisfactory results. Likewise, the check process was completed via the problem addressed by Ampofo and Karayiannis [25]. It consists on a 2D-ended square cavity filled with air and differentially heated between the vertical walls in turbulent regime. To deal with such a benchmark case, the following dimensionless parameters were used: $Pr = 0.71$ and $Ra_T = 1.58x10^9$. The results are shown in Fig. 2 for dimensionless temperature, *W*-velocity plotted at $Z = 0.5$, and local Nusselt number at the cold and hot walls. It can be seen that the results match those obtained experimentally [25]. Under these comparisons, we can conclude that the implemented approach shows satisfactory results.

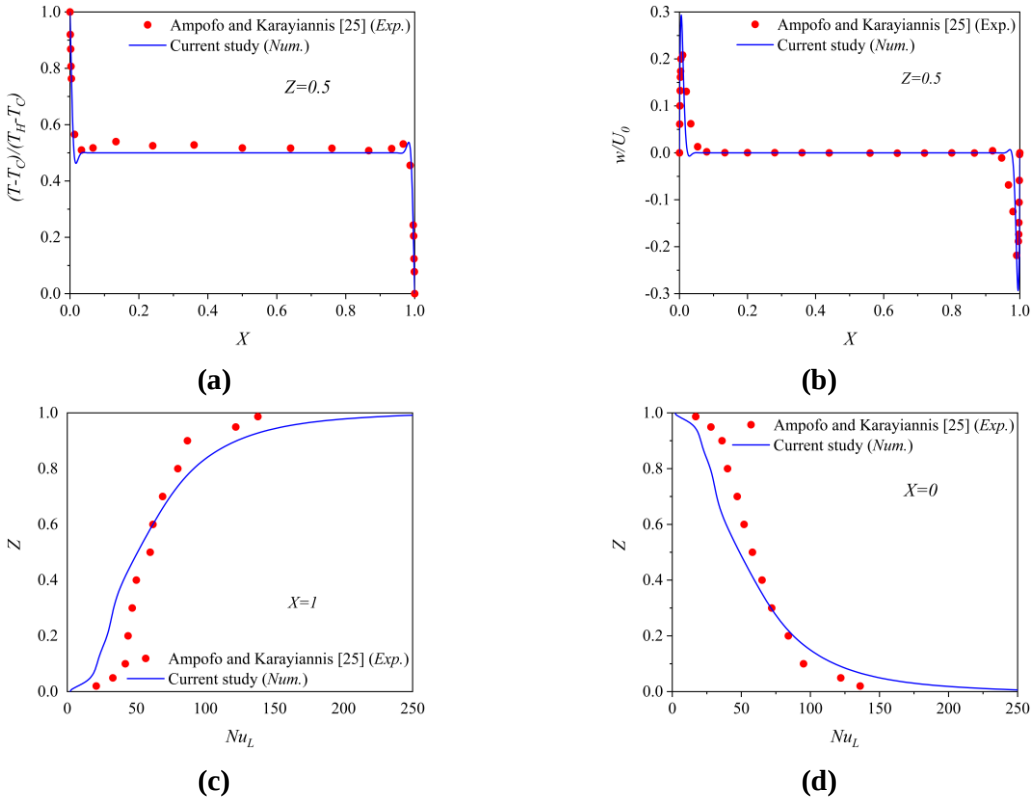

Figure 2. Comparison with Ampofo and Karayiannis [25]: (**a**) dimensionless temperature, (**b**) dimensionless w-velocity, (**c**) Nu_l at the cold wall, and (**d**) Nu_l at the hot wall; with $Ra_T = 1.58x10^9$.

4. Results and discussions

In the following, we present the results of 2D-ventilated square cavity heated from below, and filled with an air-CO_2 mixture (Pr = 0.71). The heights of the air inlet and outlet openings are h_{in} = 0.018 *m* and h_{out} = 0.024 *m*. The air-CO_2 mixture penetrates at 288 *K* and 350 *ppm* with a velocity of 0.57 ms^{-1}. The vertical walls and the upper one are maintained at a uniform temperature and CO_2-concentration of 288 *K* and 350 *ppm*, respectively. The lower wall is attached a constant temperature (T_H = 308.5 *K*) and CO_2-concentration (C_H > 350 *ppm*). The obtained Reynolds and thermal Rayleigh numbers are equal to $2.62x10^9$ and 706, respectively. It is useful to recall that, in the case of displacement ventilation, forced convection is generally low. Buoyancy forces due to the difference of temperature and concentration affect the flow. The presence of these forces creates mixed convection which can occur with different magnitudes. To quantify this, the Richardson number that represents the ratio between the natural and forced convections ($Ri = (Ra_T/Pr)/Re^2$, where Ra_T and Re being defined with the same scale L) was defined. When Ri = 1, the two forces are equivalent and the developed flow is mixed convective. Depending on the range wherein the problem is defined $0 < Ri < 1$ or $1 < Ri < \infty$, the natural and forced convection forces are present with a different interaction. For $Ri >> 1$, the flow is only driven by the free convection, while for $Ri << 1$, forced convection prevails. From the obtained Richardson number (Ri = 2.23), the flow is mixed convective with a slight dominance of free convection.

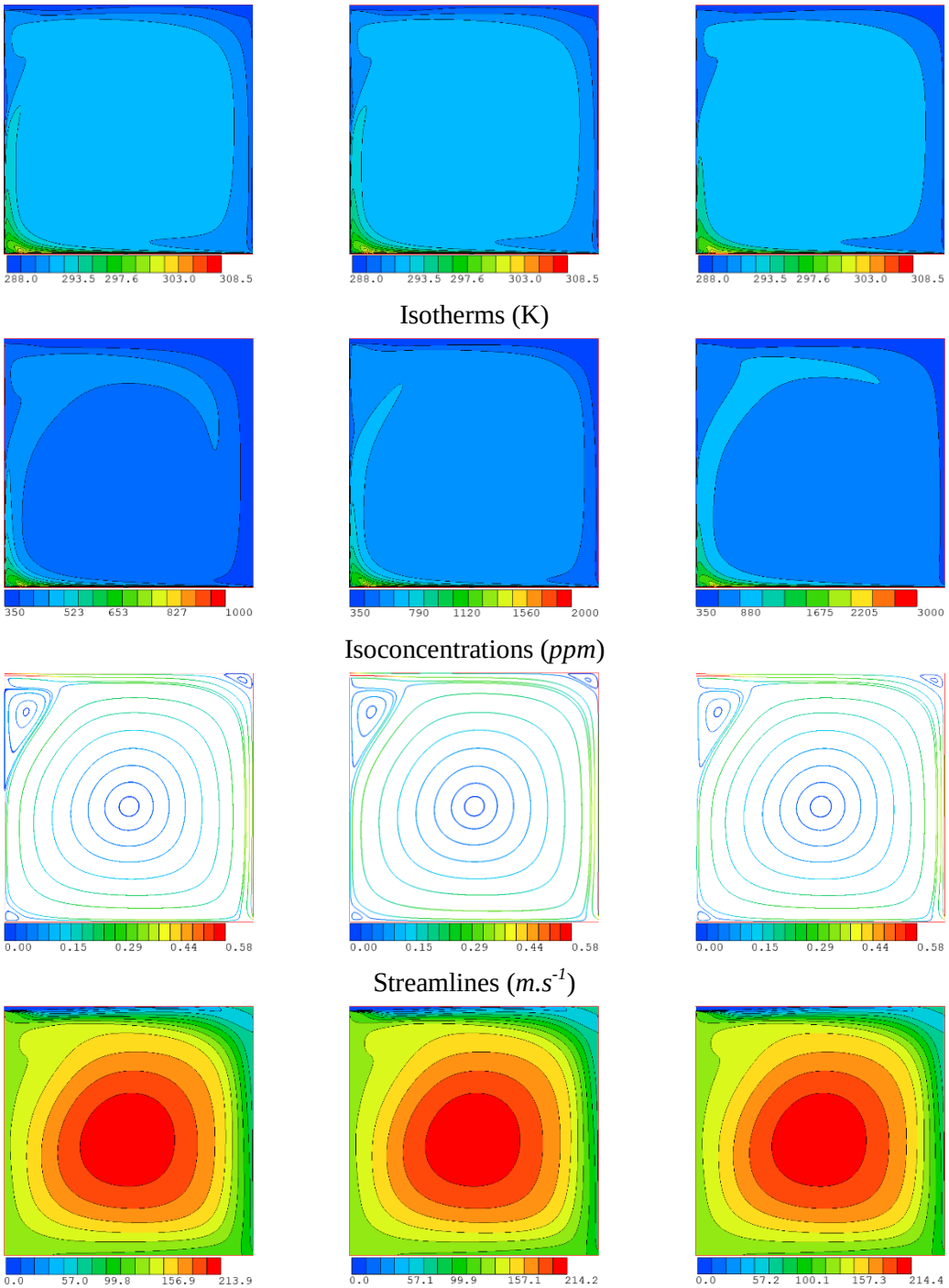

Figure 3. Isotherms, iso-concentrations, streamlines and age of air: (left) C_H = 1000 *ppm*, (middle) C_H = 2000 *ppm* and (right) C_H = 3000 *ppm*.

4.1. Flow patterns

To identify the flow behavior, and the distribution of temperature and CO_2-concentration inside the cavity, it is important to know how the fresh air is distributed in the cavity. For this, we illustrate isotherms, CO_2-isolines, streamlines and age of air in Fig. 3 for different values of C_H (1000, 2000 and 3000 *ppm*). It should be noted that the corresponding buoyancy ratios (N) are -3.12×10^{-3}, -7.93×10^{-3}

and -1.25x10^{-2}, respectively. It is worth noting that the flow is opposing when N is negative. Simply stated, the solutal buoyancy force opposes that of thermal buoyancy force.

Regarding isotherms, it is observed that the cold air becomes warm as it comes near the bottom. Then, it rises towards the cavity upper part. During this movement, the heat is trapped in the center of the cavity with some thermal stratification in the heart of the cavity while explaining the resting state of the fluid in this area. It should be noted that the isotherms are insensitive to the increasing of the CO_2 source (C_H) due to the low values of buoyancy ratios. This means the solutal buoyancy forces are negligible past the thermal buoyancy and external forces are the motor of the motion. As for the CO_2-isolines, they follow the isotherms but the quantity of CO_2 increases as C_H growing. For streamlines, we observe a large recirculation vortex in the cavity, which is driven by the jet and buoyancy forces. In addition, two smaller structures are distinguished in the upper right corner and the lower left one. The flow pattern for three C_H values appears to be almost identical for the same reason mentioned above. Also, we note the emergence of a third cell close to the inlet port and below the jet. This is due to the Coanda effect and interaction between natural and forced convections. To get an idea about the time what fresh air takes to sweep the cavity, the local age of air [26] is presented. We found that fresh air takes less time to get closer to walls due to the closure of the flow at these locations. In the middle of the cavity, air passes over time due to prevailing low velocities at the center of cavity. Regarding the results obtained, there was no change in the airflow and thermal behavior when C_H increases. This is due to the low contribution of the solutal buoyancy forces (the ratio N being close to zero).

To determine the value of C_H for which the flow physics is affected by solutal convection, we have performed a numerical experiment by increasing C_H to 2x10^4 *ppm*. Fig. 4 illustrates the temperature, u- and w-velocity components, and intensity of turbulent kinetic energy profiles along the vertical and horizontal mid-planes for C_H equal to 10^3, 3x10^3 and 20x10^3 *ppm*. We observe that the velocity components and temperature do not change with C_H. Although, the intensity of the turbulent kinetic energy is slightly sensitive when C_H = 20x10^3 *ppm.* This confirms what has been said above. As conclusion, the effect of solutal convection is negligible in the building scale due to the low CO_2-concentrations, but remains dangerous to human being health beyond a certain threshold concentration (10^3 *ppm*, in France). It may be advisable to consider the effect of CO_2 density in industrial processes where concentrations are much higher (e.g. combustion process).

The analysis of Fig. 5 shows that the increasing of C_H causes an increase of the CO_2-concentration in the large central part of the cavity. It ranges from about 430 *ppm* for C_H = 10^3 *ppm* to 850 *ppm* when C_H = 3x10^3 *ppm*. The CO_2-contaminant profiles plotted along the cavity bisector indicate that the CO_2 is homogeneous in the occupied zone and all concentration gradients are located near walls. This demonstrates that there is no concentration pic that can harm occupants' health.

Table 3 shows the mean temperature (T_m) and CO_2-concentration (C_m), and their standard deviation (σ) within the cavity according to the C_H. We see clearly that T_m is insensitive to the increasing of C_H (σ = 0 *K*). In the other hand, CO_2-concentration is highly increased by C_H, σ is important (201.5 *ppm*). This is due to the increasing of the CO2 source amount. The standard deviation σ is obtained via the relationship:

$$\sigma = \sqrt{\sum_{i=1}^{N} \frac{1}{N} \left(\phi_i - \bar{\phi} \right)^2} \qquad (1)$$

with ϕ_i is the discrete variable, $\bar{\phi}$ is the average value, and N is the number of observations.

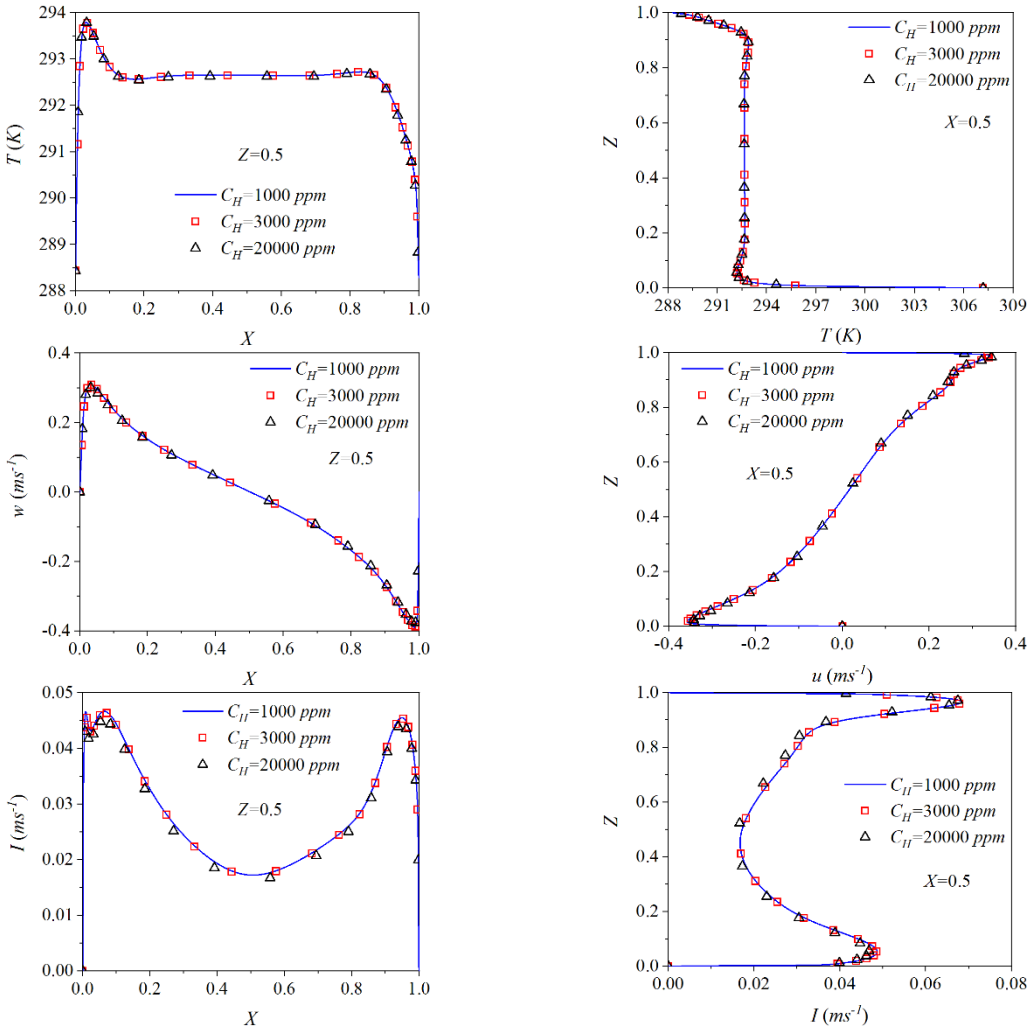

Figure 4. Contour plots along the horizontal and vertical cavity bisectors: (top) temperature, (center) w- and u-profiles, and (bottom**)** turbulent kinetic energy intensity ($I = \sqrt{k}$), with different values of C_H; (left) Z = 0.5 and (right) X = 0.5.

Table 3. Mean internal temperature and CO_2-concentration and their standard deviation (σ).

C_H (ppm)	T_m (K)	C_m (ppm)
$1x10^3$	292.5	427.5
$2x10^3$	292.5	631.3
$3x10^3$	292.5	830.6
σ	0.0	201.5

4.2. Nusselt and Sherwood numbers on the hot wall

To quantify the convective heat and mass transfers, one often uses the local and average Nusselt and Sherwood numbers. Here, both are defined as:

$$Nu_m = \frac{1}{L}\int_0^L \left(Nu_l\right)_{z=0} dx = \frac{-1}{L\Delta T}\int_0^L \left(\frac{\partial T}{\partial z}\right)_{z=0} dx \tag{2}$$

$$Sh_m = \frac{1}{L}\int_0^L \left(Sh_l\right)_{z=0} dx = \frac{-1}{L\Delta C}\int_0^L \left(\frac{\partial C}{\partial z}\right)_{z=0} dx \tag{3}$$

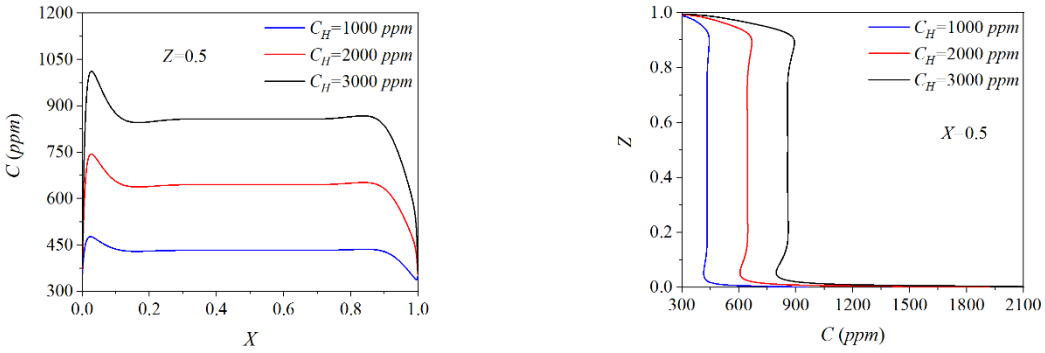

Figure 5. CO_2-concentration plots along the cavity bisectors: (left) Z = 0.5 and (right) X = 0.5.

The local and averaged Nusselt and Sherwood numbers on the hot wall (bottom wall) for a wide range of C_H graphically depicted in Fig. 6. We observe that, at the outside of the vertical boundary layers, Nu_l is minimum near the left wall (air-CO_2 mixture is hot) and increases to its maximum at the opposite wall (air-CO_2 mixture is cold) (see Fig. 6a). As a function C_H, Nu_l is identical because the variations of buoyancy ratio are very low. Regarding the local Sherwood number (Fig. 6b), Sh_l has a similar evolution compared to Nu_l with a slightly higher values and decreases softly when C_H increases. As for average Nusselt and Sherwood numbers (Fig. 6c), Nu_m remains stable when C_H increases, in contrary Sh_m which decreases. Based on these results, we conclude that solutal buoyancy forces do not contribute to the enhancement of heat and mass transfers.

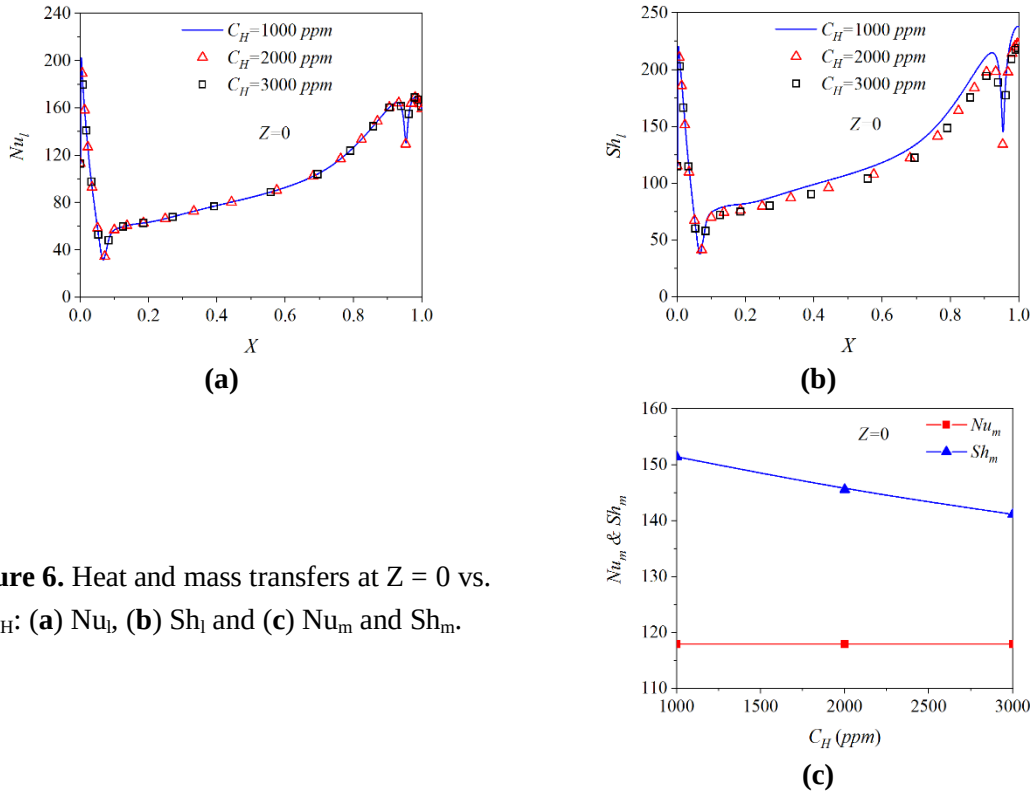

Figure 6. Heat and mass transfers at Z = 0 vs. C_H: (**a**) Nu_l, (**b**) Sh_l and (**c**) Nu_m and Sh_m.

4.3. Characteristic parameters

In this section, the ventilation effectiveness for temperature distribution (ε_T) and removal of CO_2-pollutant (ε_C), and index of indoor air quality (I_{IAQ}) are analyzed for the mentioned parameters and boundary conditions. These parameters are relevant to get an information on the ventilation effectiveness to ensure the occupants comfort. They provide a quantitative index related to the way in

which heat and pollutants are distributed all over inside the cavity, the higher the value is, the more homogeneous temperature and pollutants distributions are. Awbi expresses this parameter as [27]:

$$\varepsilon_T = \frac{T_{out} - T_{in}}{T_m - T_{in}} \tag{4}$$

$$\varepsilon_C = \frac{C_{out} - C_{in}}{C_m - C_{in}} \tag{5}$$

$$I_{IAQ} = \frac{C_m - C_{out}}{C_{Th} - C_{out}} \tag{6}$$

Four configurations were considered: Configuration A (inlet gap on the upper of the left wall and outlet on the lower of opposite wall; Fig.1), Configuration B (inlet gap on the lower of the left wall and outlet on the upper of the opposite wall), Configuration C (inlet opening on the lower part of the left side and outlet on the upper of the same side), and Configuration D (inlet on the upper of the left side and outlet on the lower of the same side). The obtained results are gathered in table 4 vs. C_H.

Table 4. ε_T, ε_C, and I_{IAQ} values vs. C_H.

C_H (*ppm*)	ε_T	ε_C	I_{IAQ}	*Configuration*
$1x10^3$	0.71	0.63	0.05	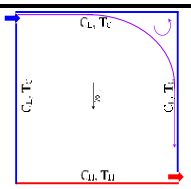
$2x10^3$	0.71	0.72	0.18	
$3x10^3$	0.71	0.73	0.45	
$1x10^3$	0.81	1.10	-0.01	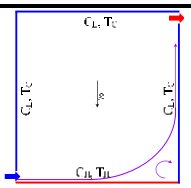
$2x10^3$	0.81	1.14	-0.05	
$3x10^3$	0.81	1.24	-0.23	
$1x10^3$	0.73	0.94	0.00	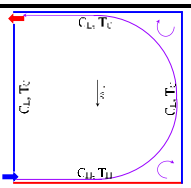
$2x10^3$	0.73	1.09	-0.03	
$3x10^3$	0.73	1.14	-0.13	
$1x10^3$	4.68	5.79	-0.16	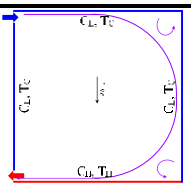
$2x10^3$	4.68	8.86	-0.96	
$3x10^3$	4.69	11.79	-6.56	

The results show that ε_T is not affected by the increase of C_H for the reasons up-mentioned indicating that solutal buoyancy forces do not induce changes in heat and mass transfers. Regarding the pollutant removal effectiveness, it is found that ε_C evolves with C_H. It was found that the configuration D provides the highest value of ε_T and ε_C compared to the others. As can be seen, the values remain significantly larger than unity indicating that the ventilation sufficiently evacuate the heat and the CO_2-contaminant. In terms of indoor air quality, I_{IAQ} is less than unity for all configurations and C_H values considered meaning they all ensure good air quality. Nevertheless, the configuration D provides the best performance. It is worthy to note that the sign (-) indicates that the

CO_2-concentration at the outlet gap (C_{out}) is greater than the average CO_2-concentration of the cavity (C_m).

Based on the obtained results, it may be concluded that the configurations A, B and C uphold ε_T and ε_C close to unity and I_{IAQ} less than unity. Thereby, they can be used in temperate climate zones (e.g., Mediterranean climate) to ensure an acceptable IAQ and maintaining an appreciable temperature level. As for the configuration D, it can be used to remove the internal heat while contributing to refresh the room in summer and insure a good IAQ.

5. Conclusions

The low-turbulent double-diffusive mixed convection flow in a 2D-ventilated room filled with an air-CO_2 mixture was computationally investigated. The emphasis has been on the CO_2-diffusion effect on the flow behavior, temperature distribution and indoor air quality. Computations have been performed with thermal Rayleigh number of 2.62×10^9, Reynolds numbers of 706, Prandtl number of 0.71, Lewis number of 1.47, and various CO_2 source between 10^3 and 3×10^3 *ppm*. In RANS equations, the RNG k-ε turbulence model was used. Based on the simulation results, our main findings can be drawn as follows:

- The analysis of the effect of CO_2-diffusion showed that solutal convection can be neglected in the field of building because the CO_2-concentration level is low but still dangerous. It is recommended to consider its effect on industrial applications where concentrations are heavy;
- Regarding heat and mass transfers, the increasing of CO_2 amount does not improve or demean both Nusselt and Sherwood numbers due to the low buoyancy ratios, which are closely zero;
- In terms of thermal comfort, the configuration D exhibits a much higher ε_T (>unit) than that of other configurations. Thereby, it seems to be intended to evacuate sufficient internal heat, and may be suitable for use in summer. As for configurations A, B and C, they present a ε_T close to unity and can, therefore, be used in winter in temperate climates for the CO_2 release;
- Finally, from the results of the ventilation efficiency for the removal of pollutant (ε_C) and the indoor air quality index (I_{IAQ}), it was found that the mixing ventilation process uphold an acceptable and homogeneous CO_2-concentration distributions, and that all configurations ensure an appreciable indoor air quality based on the CO_2-pollutant.

Nomenclature

C	Chemical species' concentration (kgm^{-3} or ppm)	β_T	Thermal expansion coefficient (K^{-1})
C_{Th}	Threshold concentration (kgm^{-3} or ppm)	ΔC	Characteristic concentration difference, $\Delta C = (C_H - C_L)$ (kgm^{-3})
D	Diffusion coefficient (m^2s^{-1})	ΔT	Characteristic temperature difference, $\Delta T = (T_H - T_C)$ (K)
g	Gravity acceleration (ms^{-2})	ε	Turbulence energy dissipation (m^2s^{-3})
h	Height of the inlet or outlet air gap (m)	ε_C	Ventilation effectiveness for pollutants removal (--)
H	Cavity's height (m)	ε_T	Ventilation effectiveness for temperature distribution (--)
I	Turbulent kinetic energy intensity (ms^{-1})		
I_{IAQ}	Indoor air quality index (--)		
k	Turbulent kinetic energy (m^2s^{-2})		
L	Cavity's width (m)		
Le	Lewis number, $Le = \alpha_0/D$		

N	Buoyancy ratio, $N = \beta_S \Delta C / \beta_T \Delta T$
Nu	Nusselt number (--)
p	Fluid pressure (Pa)
Pr	Prandtl number, $Pr = \nu_0/\alpha_0$
Ra_T	Rayleigh number, $Ra_T = g\beta_T \Delta T H^3/(\nu_0 \alpha_0)$
Re	Reynolds number, $Re = \rho_0 U_{in} h_{in}/\mu_0$
Ri	Richardson number, $Ri = (Ra_T/Pr)/Re^2$
Sh	Sherwood number (--)
T	Fluid temperature (K)
u, w	Horizontal and vertical velocities (ms^{-1})
U	Velocity modulus (ms^{-1})
U_0	Buoyancy velocity, $U_0 = \sqrt{g\beta_T \Delta T H}$ (ms^{-1})
x, z	Horizontal and vertical coordinates (m)
X, Z	Dimensionless coordinates, $(X, Z) = (x, z)/H$

Greek Symbols

α	Thermal diffusivity ($m^2 s^{-1}$)
β_S	Solutal expansion coefficient ($m^3 kg^{-1}$)
μ	Dynamic viscosity ($kgm^{-1}s^{-1}$)
ν	Kinematic viscosity ($m^2 s^{-1}$)
ρ	Density (kgm^{-3})
σ	Standard deviation

Superscripts/subscripts

C	Cold
H	High or Hot
in	Inlet
L	Low
l	Local
m	Mean or average
max	Maximum
min	Minimum
out	Outlet
S	Solutal
T	Thermal
0	Reference

References

[1] Deng, Q.-H., et al., Fluid, heat and contaminant transport structures of laminar double-diffusive mixed convection in a two-dimensional ventilated enclosure, *International Journal of Heat and Mass Transfer*, *47* (2004), 24, pp. 5257-5269.

[2] Marchand, C., et al., Aldehyde measurements in indoor environments in Strasbourg (France), *Atmospheric Environment*, *40* (2006), 7, pp. 1336-1345.

[3] Kabir, E., et al., Indoor air quality assessment in child care and medical facilities in Korea, *Environmental Monitoring and Assessment*, *184* (2012), 10, pp. 6395-6409.

[4] Xamán, J., et al., Effect of a contaminant source (CO_2) on the air quality in a ventilated room, *Energy*, *36* (2011), *5*, pp. 3302-3318.

[5] Serrano-Arellano, J., et al., Optimum ventilation based on the ventilation effectiveness for temperature and CO_2 distribution in ventilated cavities, *International Journal of Heat and Mass Transfer*, *62* (2013), pp. 9-21.

[6] Liu, D., et al., Turbulent transport of airborne pollutants in a residential room with a novel air conditioning unit, *International Journal of Refrigeration*, *35* (2012), 5, pp. 1455-1472.

[7] Cao, S.-J., Meyers, J., On the construction and use of linear low-dimensional ventilation models, *Indoor Air*, 22 (2012), *5*, pp. 427-441.

[8] Cao, S.-J., Meyers, J., Influence of turbulent boundary conditions on RANS simulations of pollutant dispersion in mechanically ventilated enclosures with transitional slot Reynolds number, *Building and Environment*, *59* (2013), pp. 397-407.

[9] Deng, H.-Y., et al., Influence of air change rates on indoor CO_2 stratification in terms of Richardson number and vorticity, *Building and Environment*, *129* (2018), pp. 74-84.

[10] Saha, S., et al., Double diffusive mixed convection heat transfer inside a vented square cavity, *Chemical Engineering Research Bulletin*, *13* (2009), 1, pp. 17-24.

[11] Abidi A., et al., Effect of heat and mass transfer through diffusive walls on three-dimensional double-diffusive natural convection, *Numerical Heat Transfer, Part A, 53* (2008), pp. 1357-1376.
[12] Abidi A., et al., Effect of radiative heat transfer on three-dimensional double diffusive natural convection, *Numerical Heat Transfer, Part A, 60* (2011), pp. 785-809.
[13] Ahmed K .H., et al. Three-dimensional unsteady natural convection and entropy generation in an inclined cubical trapezoidal cavity with an isothermal bottom wall, *Alexandria Engineering Journal, 55* (2016), pp. 741-755.
[14] Krajčík M., et al., Air distribution and ventilation effectiveness in an occupied room heated by warm air, *Energy and Buildings, 55* (2012), pp. 94-101.
[15] Rodríguez-Muñoz, N. A., et al., Numerical study of heat transfer by convection and thermal radiation in a ventilated room with human heat generation and CO_2 production, *Latin American Applied Research, 43* (2013), pp. 353-361.
[16] Serrano-Arellano, J., et al., Indoor air quality analysis based on the ventilation effectiveness for CO_2 contaminant removal in ventilated cavities, *Revista Mexicana Física*, 60 (2014), 4, pp. 309-317.
[17] Serrano-Arellano, J., et al., Numerical investigation of transient heat and mass transfer by natural convection in a ventilated cavity: Outlet air gap located close to heat source, *International Journal of Heat and Mass Transfer, 76* (2014), pp. 268-278.
[18] Blay, D., et al., Confined turbulent mixed convection in the presence of a horizontal buoyant wall jet, *ASME Fundamentals of Mixed Convection HTD, 213* (1992), pp. 65-72.
[19] Poling, B. E., et al., *The properties of gases and liquids*, 5th Ed. McGraw-Hill, NewYork, USA, 2001.
[20] Koufi, L., et al., Numerical investigation of turbulent double-diffusive mixed convection in a slot ventilated enclosure with supply air flow ports, 23ème Congrès Français de Mécanique, 2017, Lille, France.
[21] Koufi, L., et al., Numerical investigation of turbulent mixed convection in an open cavity: Effect of inlet and outlet openings, *International Journal of Thermal Sciences, 116* (2017), pp. 103-117.
[22] Koufi, L., et al, Double-diffusive natural convection in a mixture-filled cavity with walls' opposite temperatures and concentrations, *Heat Transfer Engineering, 40* (2018), 15, pp. 1-18.
[23] Koufi, L., et al., A numerical study of indoor air quality in a ventilated room using different strategies of ventilation, *Mechanics and Industry, 18* (2017), 2, pp. 1-9.
[24] Younsi, Z., et al., Numerical study of the effects of ventilated cavities outlet location on thermal comfort and air quality, *Int. J. of Numerical for Methods for Heat and Fluid Flow, 29* (2019), 11, pp. 4462-4483.
[25] Ampofo, F., Karayiannis, T. G., Experimental benchmark data for turbulent natural convection in an air-filled square cavity, *International Journal of Heat and Mass Transfer, 46* (2003), 19, pp. 3551-3572.
[26] Cao, G., et al., A review of the performance of different ventilation and airflow distribution systems in buildings, *Building and Environment, 73* (2014), pp. 171-186.
[27] Awbi, H. B., *Ventilation of buildings*, 2nd ed. Routledge, New York, USA, 2003.

Received: 16.1.2020.
Revised: 31.8.2020.
Accepted: 22.9.2020.